Formation of layer structures in H_2SO_4 intercalated poly(*p*-phenylene vinylene)

Guomin Mao and M. J. Winokur
Department of Physics, University of Wisconsin, Madison, Wisconsin 53706

F. E. Karasz
Department of Polymer Science and Engineering, University of Massachusetts, Amherst, Massachusetts 01003

(Received 24 February 1998)

X-ray-diffraction studies of highly oriented poly(*p*-phenylene vinylene) (PPV) films before and after vapor-phase or liquid-phase intercalation by H_2SO_4 have been performed. In both cases the data support a structural evolution dominated by a direct transformation of the original PPV polymer to a single, heavily doped phase. The best-fit model obtained from structure-factor refinements to the H_2SO_4-PPV equatorial data is fully consistent with the previously proposed ''stage-1'' layered structure in which the PPV chains and the sulfate ions form an alternating sequence of cation- and anion-radical layers with a monoclinic unit cell dominated by the PPV placement and lattice parameters of $a=9.98$ Å, $b=6.80$ Å, $c=6.6$ Å, and $\gamma=94.5°$. Nonequatorial scattering data suggest that at room temperature the H_2SO_4 layer is not well ordered. Additional data sets probing the anisotropy within the equatorial plane (perpendicular to the PPV chain axis) clearly indicate that the insertion of H_2SO_4 layers occurs by creating galleries that are parallel to **a**-**c** plane of the PPV host polymer. This direction is effectively *perpendicular* to the commonly accepted intercalation scheme, which has these layers parallel to the pristine PPV [100] planes. [S0163-1829(98)08231-9]

I. INTRODUCTION

Understanding the underlying mechanisms by which π-conjugated polymer hosts accommodate various intercalant species into the host matrix has remained an important issue for fundamental reasons as well as for more application oriented goals.[1,2] At the most core level are basic questions concerning the nature of structural evolution in systems manifesting competing interactions. In the case of polymers the structural evolution is always constrained by the nature of the host wherein there is strong covalent bonding along the polymer chain axis and weaker interactions in the orthogonal directions. Superimposed on this framework is the strong electron-lattice coupling along the polymer chain axis, which gives rise to the unusual charge transport properties. This picture is further complicated after intercalation by a guest species (or dopant) that creates disruptive rotational and translational displacements of the host matrix in order to facilitate intercalant uptake. While the quasi-one-dimensional electronic excitations originally garnered the most attention, many physical properties and most envisioned conducting polymer applications are mediated by the full three-dimensional structure occurring on a myriad of length scales. Thus a detailed knowledge of the molecular organization is a fundamental starting point for obtaining a more complete perspective.

At present the most developed molecular-level structural picture pertaining to poly(*p*-phenylene vinylene) (PPV) and other crystalline linear conducting polymers [e.g., polyacetylene or poly(*p*-phenylene)] are generally limited to the smallest intercalant species (i.e., alkali metals) and the evolution to a quasi-one-dimensional channel structure.[3–14] In these situations the structural transformation is often dominated by rotations about the polymer chain axis. This response is responsible for the appearance of periodic arrays of one-dimensional channels parallel to the polymer chain axes that are densely filled by the constituent alkali-metal ions. As the projected equatorial representations in Fig. 1 show, both threefold and fourfold channel structures are commonly observed depending on the relative guest-host sizes and compositions. In the specific case of hosts whose equatorial packing nearly approximates a triangular lattice, much of the underlying structural behavior seen when using smaller alkali-metal guests is reflected in the phase diagrams obtained from mean-field studies of the generalized anisotropic planar rotor model of Choi, Harris, and Mele.[15–17] For systems employing somewhat larger alkali-metal species, intercalant uptake involves significant rotational and translational displacements with the formation of tetragonal and orthorhombic phases,[3,10] although there is other evidence for more complex structural forms.[8,14] In either case the free volume available within the polymer matrix is sufficient so that the overall space occupied by the composite material is nearly the same as that of the pristine PPV host itself[13] and the loss in the measured crystal coherence lengths is minimal. In this context the intercalation process in channel forming compounds may be viewed as only moderately disruptive.

In contrast, the structures induced by the larger, anion-radical forming molecular (*p*-type) dopant species (e.g., H_2SO_4 and AsF_5) are generally thought to be dominated by the creation of two-dimensional (2D) galleries of guest anions separated by a single stacked layer of the positively charged polymer host chains.[18–22] In this way the polymer host layer is seen to maintain π stacking so that interchain transport properties are enhanced with, in some instances, the appearance of metalliclike behavior.[23,24] In the current situation the structural evolution of this layered phase is often cast in direct analogy to that of quasi-2D intercalation compounds[25,26] whereby a ''stage-1'' layer compound occurs by direct insertion of the intercalant between preexisting

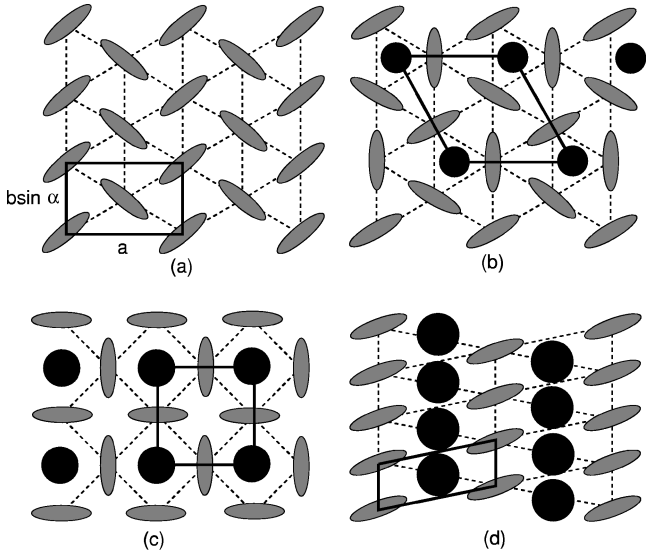

FIG. 1. Various template structures for the equatorial packing of (a) crystalline PPV and three representative intercalated phases having (b) a threefold channel structure, (c) a fourfold channel structure, and (d) a stage-1 layered structure. The ellipses represent the polymer host chains, while the solid black circles indicate occupied intercalant galleries.

stacks of the polymer chains.[21,27–29] In the case of conducting polymers and especially in PPV, which has appreciable axial ordering within the **b**-**c** plane (see Fig. 2), the natural inclination is to present a model in which the molecular anion layer opens galleries parallel to the [100] planes of the PPV host as depicted in Figs. 3(a) and 3(b). The wholesale insertion of these molecular anion-radical layers involves enormous changes in the lateral dimensions and location of the polymer chains with significant increases in the average 2D equatorial area per polymer chain. In addition, *p*-type doped systems often exhibit significant broadening in the observed diffraction peak widths indicative of an overall reduction in the estimated crystallite coherence lengths.

In this paper we present x-ray scattering data and modeling analysis of H_2SO_4-doped PPV samples that suggest that, while a lamellar structure is fully consistent with the experimental data, the intercalation process itself actually involves a counterintuitive reconstruction in which the PPV chains undergo a disruptive sequence of translational displacements with insertion of layers normal to the PPV (010) direction as shown in Figs. 3(c) and 3(d). This direction is *perpendicular* to the one that has been inferred in prior schematic representations. Hence the naive one-to-one mapping of the polymer intercalation processes to that occurring in layered materials must be carefully reassessed. This surprising mechanism may also explain why higher-order layered stages are not generally observed and why the intercalation process often produces layered materials with drastically reduced peak widths and coherence lengths.

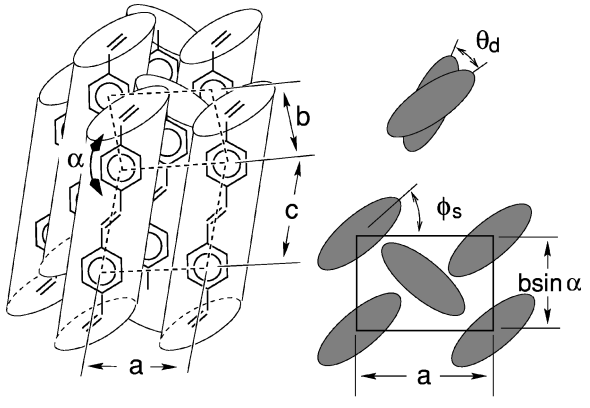

FIG. 2. Left: sketch of the PPV chain structure and the crystalline three-dimensional packing. The unit cell is reported to be monoclinic with lattice constants of approximately $a=7.8$ Å, $b=5.1$ Å, $c=6.6$ Å, and $\gamma=135°$ (from Refs. 31,39). Right: alternate views of the 2D projection identifying the single chain degrees freedom referred to as the setting angle ϕ_s and the phenylene ring nonplanarity θ_d.

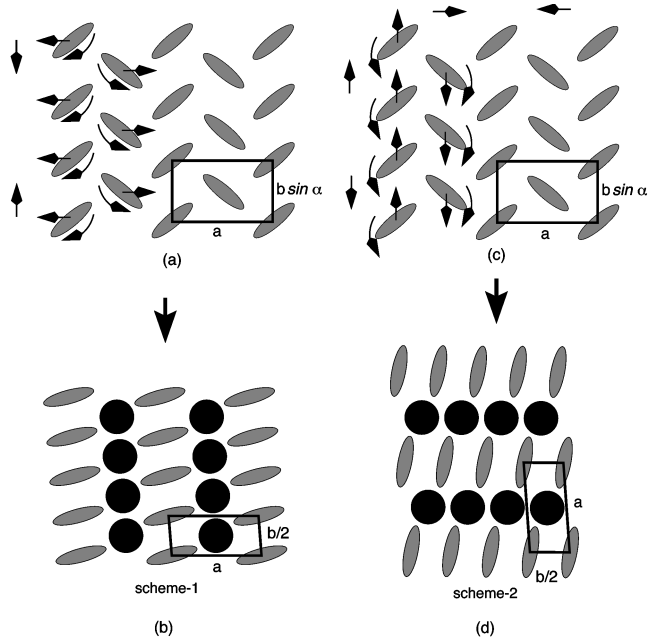

FIG. 3. Projected equatorial views of PPV undergoing the transformation to the stage-1 layer phase via insertion of H_2SO_4 layers (a) and (b) perpendicular to the [100] direction and (c) and (d) perpendicular to the $b\sin\alpha$ direction.

II. EXPERIMENTAL DETAILS

The PPV films used in this study were prepared by a precursor route whereby the soluble precursor polymer,[30] poly(*p*-xylene-α-dimethylsufonium chloride), was initially cast from solution into films and then simultaneously uniaxially stretched and thermally converted by passing these films over differentially driven, heated rollers. This processing yields moderately crystalline materials with the polymer chain axis oriented highly parallel to the stretching direction. The mechanical processing also imparts additional ordering in the direction perpendicular to the polymer chain axis so that a full three-dimensional texture is obtained.[31] In general there is a multimodal distribution of crystallites about the *c* axis. Once formed, the oriented PPV films are additionally annealed at higher temperature (approximately 280 °C) to fully complete the conversion process and further improve the crystallinity. Coherence lengths ranging between 150 and

200 Å, in both the equatorial and the meridional directions, represent typical upper limits.

Two different intercalation methods were employed. Previously prepared single-layer PPV films (approximately 5 μm thick) were placed into standard borosilicate test tubes. For vapor-phase doping a small quantity of sulfuric acid (98% H_2SO_4, J. T. Baker) was added to the test tube. Afterwards this tube was evacuated to a pressure of approximately 10^{-3} Torr, sealed, and then mounted into a simple two-zone furnace. The temperatures of the H_2SO_4 and PPV film samples were maintained near 50 °C and 60 °C, respectively. The time required to obtain single phase samples was found to be highly variable with 24 h of exposure a typical lower limit. We note that PPV films annealed for extended times at high temperature achieve better sample crystallinity, albeit with poorer dopant diffusion rates and increased doping times. Other samples were prepared in a N_2-gas filled glove bag by direct immersion in the H_2SO_4 liquid for a period of not less than 24 h. After this treatment most of the residual H_2SO_4 adhering to the film surface was eliminated by repeated washing in a toluene solvent bath. Once these H_2SO_4-PPV films were washed and dried they were folded or rolled into multilayer stacks, clamped, and then mounted directly onto a standard goniometer head in a He atmosphere or, alternatively, first sealed in x-ray capillaries and then mounted. Planar stacks preserve the equatorial anisotropy while rolled samples were used to mechanically generate a 2D equatorial ''powder average.''

The x-ray scattering data was recorded on one of two available diffractometers attached to a 15-kW rotating anode x-ray generator fitted with a copper target (Cu K_α, $\lambda = 1.542$ Å). Two sets of conventional θ-2θ scans were typically executed.[31,32] For the first set of scans the sample was maintained in a symmetrical transmission geometry and the orientation of the **c**-axis direction, with respect to the direction *normal* to the scattering plane swept out by the linear diode-array detector (defined as χ), was sequentially stepped from 0° up to 90°. At $\chi = 0°$ the detector probed the equatorial **a***-**b*** plane, while at $\chi = 90°$ the linear array detector was centered along the meridional direction (**c*** is *not* parallel to the **c**- or chain-axis direction in PPV). In the case of planar multifilm stacks, a second series of scans was performed with χ fixed to 0° and the PPV film stepwise rotated about the c axis from transmission to reflection geometry (again employing θ-2θ scans). In this so-called ϕ scan the textural variations within the equatorial plane could then be assessed. With $\phi = 0°$ the PPV films were maintained in a standard symmetrical transmission geometry so that the scattering vector was always parallel to this film surface (in this instance it is with respect to the central element of a short linear-array detector). By analogy a symmetrical reflection geometry (i.e., $\phi = 90°$) oriented the θ-2θ scan scattering vector normal to the film surface. From the series of sequentially stepped χ or ϕ scans a single composite x-ray isointensity contour map could be generated.

For comparison with various candidate structures the equatorial data from a cylindrically rolled sample was recorded and refined using a linked-atom least-squares algorithm incorporating standard crystallographic corrections.[33–35] Individual ($hk0$) peaks were convoluted with curves that included an arbitrary but fixed linear combination of Lorentzian and Gaussian components. The model profile was then scaled and added to an estimated background curve. The major adjustable parameters included the a, b, and γ unit cell dimensions, the chain setting angle ϕ_s (see Fig. 2), the H_2SO_4 concentration and orientation of the molecular anions, the peak widths, and an isotropic Debye temperature factor. Internal PPV chain degrees of freedom, such as deviations from rigid planarity of the phenylene rings using a twist angle θ_d and/or a root-mean-square librational parameter, were also incorporated,[36] but these produced relatively minor variations in the refined χ^2 and as such have very limited accuracy. The sulfate ion itself has a well-defined tetrahedral geometry with the sulfur at the center and oxygens at the four vertices. The O-S bond length was adjustable and refined to 1.46 Å. Since x rays do not scattering strongly from low-Z elements, the actual form of the sulfate ion and location of the hydrogen was of little consequence in the refinements. In addition, the presence of any water molecules cointercalated within the PPV matrix was also typically neglected.

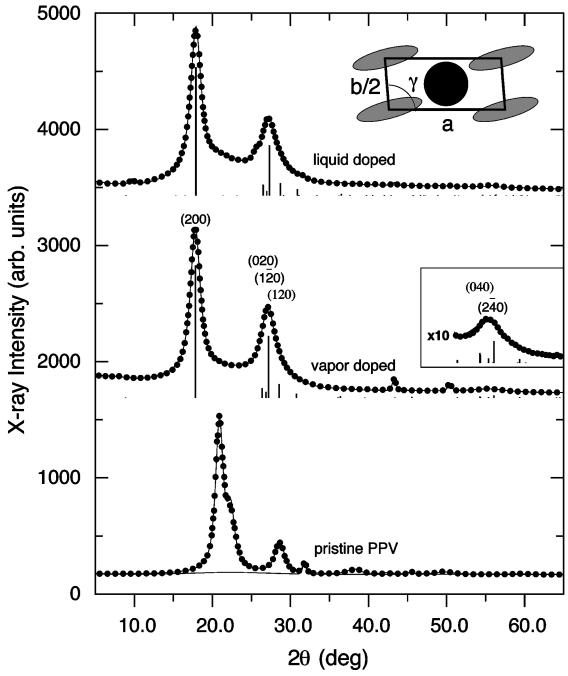

FIG. 4. Comparison of experimental ($hk0$) equatorial data (dots) in combination with the calculated profiles (solid lines) for the herringbone PPV phase and two H_2SO_4-PPV samples in the stage-1 phase. In addition, a representative background is shown in the bottom data as well and the most intense Bragg reflections (vertical lines). Inset at middle: H_2SO_4-PPV data and fit magnified a factor of 10. Inset at top: equatorial projection of the stage-1 phase.

III. RESULTS

In all samples studied, prepared using either the liquid- or vapor-phase methods, the resulting equatorial scattering profiles always indicated a simple two-phase superposition by the undoped PPV herringbone packed structure and a heavily H_2SO_4-doped PPV phase. Figure 4 displays typical equatorial ($hk0$) scans for single-phase samples after extended exposure to H_2SO_4 in combination with data from a pure PPV

film. Data from both displayed H_2SO_4-PPV films evidence a complete transformation to the stage-1 phase with no measurable PPV residue. The overall broadening of the scattering peaks and the presence of only two strong equatorial scattering features centered near 2θ values of 18° and 27° are the most pronounced attributes and are comparable to results obtained previously using alternative *p*-type dopants. The peak near 27° is noticeably broader and asymmetric and thus suggests the possibility that this feature results from a superposition of Bragg peak contributions. Sharp artifacts were always observed in both the PPV and H_2SO_4-PPV spectra. In the case of PPV these arise from crystalline NaCl residues. The analysis of the H_2SO_4 exposed films was considerably more complicated because in many instances the artifacts became quite pronounced, especially during studies performed *in situ*. The position of these sharp peaks is consistent with the formation of a variety of crystalline salts including Glauber's salt ($Na_2SO_4 \cdot H_2O$), sodium hydrogen sulfate, sodium sulfate, etc.

In addition to experimental data, Fig. 4 also contains the calculated profiles (as solid thin lines) from the best-fit models using, in the case of PPV, its well-known structure[31,37–39] as seen in Fig. 2 and, in the case of the H_2SO_4 treated samples, the oblique 2D unit cell shown in the Fig. 4 inset where the PPV chains are represented by the shaded ellipses and the sulfate anion by the solid black circle. Although a multitude of reflections yield nonzero intensities, the calculated structure factor is completely dominated by only the (200) and the $(1\bar{2}0)$ contributions. The overall lack of distinguishable features makes a definitive assignment uncertain, but, as will be shown later, this indexing is also consistent with data from samples that preserve the aforementioned equatorial anisotropy. The major calculated 2D unit cell parameters are $\mathbf{a}=9.98$ Å, $\mathbf{b}_{2D}=3.40$ Å, and $\gamma=94.5°$ with a setting angle $\phi_s \approx 15°$. The **a** repeat is slightly less than the estimated sum of the hard-core sizes along the PPV major axis (at ~6.1 Å) and that of the sulfate anion (at ~4.3 Å), a result that is consistent with the nonzero setting angle. With these parameters the nominal PPV chain-to-chain contact distance becomes nearly 3.3 Å, thus establishing a strong interchain overlap of the π orbitals and the possibility of good interchain charge transport.

Other parameters in the stage-1 structure factor refinement included a slight phenyl ring twist away from planarity of ~5° and an isotropic Debye-Waller factor of 0.3 Å^2. From the peak widths we estimate a nominal 90 Å crystal size, which is significantly less than that of the starting PPV material. The position of the sulfate tetrahedron was found to be close to the center of the 2D unit cell [at $(0.5\mathbf{a}, 0.4\mathbf{b}_{2D})$] with the tetrahedra oriented so that the four corner oxygen atoms appear equidistant from the central sulfur atom when viewed from directly above (i.e., parallel to the PPV chain axis). Translational displacements of up to 0.3 Å by the sulfate tetrahedra in the direction parallel to the **b** axis did not significantly worsen the quality of the fits after allowing for minor readjustment of various other refined parameters. In contrast, the refinements were extremely sensitive to displacements along the **a**-axis direction. The sulfate concentration per PPV monomer repeat unit (C_8H_6) was fixed at a 1:1 ratio. With one tetrahedron per unit cell this guarantees commensurability along the chain axis and simplifies the modeling process. Slight improvements in the $(hk0)$ fits were obtained by using a slightly lower sulfate composition ($\approx 10\%$). Assuming that compositions in this range are essentially correct, the additional cointercalation of water, perhaps in the form of $(H_3O)^+HSO_4^-$,[40,41] cannot be very extensive because the contribution of this water to the x-ray scattering significantly worsens the best fit. Once again we emphasize that the lack of distinguishable scattering data significantly limits the microscopic details that can be definitively extracted from this structural model.

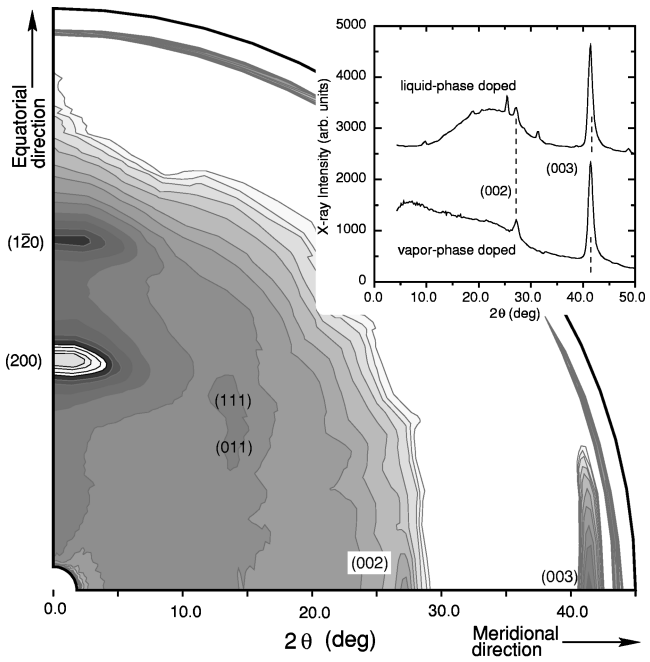

FIG. 5. Contour map of constant x-ray intensity between the PPV **c** axis and the equatorial $hk0$ equatorial plane for a vapor-phase intercalated (''doped'') H_2SO_4-PPV sample. Inset: individual diffraction profiles along the meridional direction.

The constant x-ray intensity contour map, shown in Fig. 5, reveals the nonequatorial scattering. The most obvious feature is the superposition of the relatively localized peaks from the PPV chain contributions on top of a rather diffuse background from the sulfuric acid intercalant. Meridional scans, along the *c*-axis direction with profiles as shown in the inset of Fig. 5, clearly exhibit both these sharp and broad contributions. The relatively sharp peaks, at 2θ values of 27.0° and 41.4°, occur at the intersection of $\ell=2$ and 3 layer lines from the PPV chain scattering. This yields a *c*-axis periodicity of 6.58 Å for the PPV and is comparable to the 6.64 Å seen in the pristine PPV samples. The intensity distribution of the PPV scattering is quite similar to that expected from a single PPV chain,[39] indicating very poor axial ordering, although it is, in principle, possible to index the observed data in terms of a monoclinic unit cell. These results are similar to the earlier work of Masse *et al.*[21] The relatively broad and featureless background reaches a maximum, in the case of vapor-phase doping, near $2\theta \approx 24°$ and indicates a nominal ~3.7 Å repeat for the sulfuric acid intercalant along the PPV chain direction. *Assuming* an out-of-phase nesting between sulfate tetrahedra in adjacent unit cells within each layer gallery, this results in a ~7.4 Å sul-

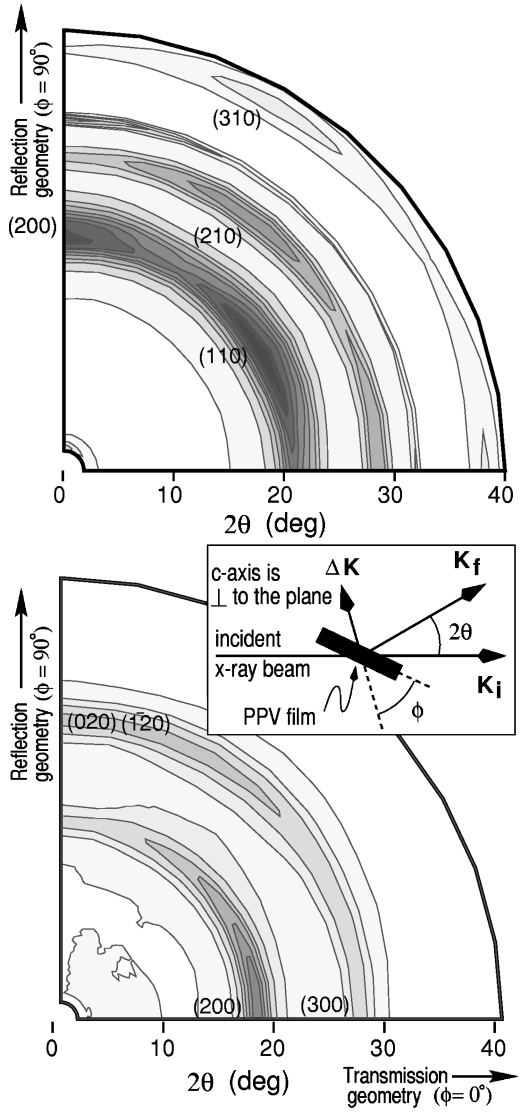

FIG. 6. Contour maps of constant x-ray intensity about the equatorial plane from transmission to reflection geometry (as shown in the inset at middle) for a pristine PPV (at top) and a H_2SO_4-PPV stage-1 sample with the approximate position of the most intense Bragg reflections assuming the equatorial anisotropy specified in the text.

fate anion repeat that generally consistent with the results from the refinement of the equatorial data (a 0.9:1 sulfuric acid/PPV ratio implies a 7.4 Å repeat of the molecular anion). Thus we arrive at a proposed PPV-H_2SO_4 monoclinic unit cell approximate of $\mathbf{a}=9.98$ Å, $\mathbf{b}=6.80$ Å, $\mathbf{c}=6.6$ Å, and $\gamma=94.5°$. The slightly more intense feature in the liquid immersed PPV film is probably indicative of some unincorporated H_2SO_4 residues. In either case, there are no scattering signatures consistent with extensive ordering at room temperature by the sulfuric acid filling the 2D intercalant galleries.

The two constant x-ray intensity contour maps shown in Fig. 6 for pristine PPV and a H_2SO_4-PPV sample reveal the structural anisotropy within the equatorial plane. In the pristine PPV scan the anisotropy within the $\mathbf{a}^*$-$\mathbf{b}^*$ plane is sufficiently pronounced that a clear identification of the most intense scattering features is possible. The actual distribution of the PPV crystallites is trimodal,[31] with nearly 50% of the crystallites situated with their *a* axes oriented on average perpendicular to the film surface. The indexing of the contour maps is keyed to this dominant component. In addition, there are two more Gaussian centroids, each representing nearly 25% of the film crystallites with their *a* axes oriented approximately $\pm 60°$ from the surface normal. A simple θ-2θ scan using a transmission geometry probes structure parallel to the film surface (and therefore the most prevalent fraction of PPV crystallites along the $\mathbf{b}^*$ direction of the PPV unit cell), while a scan in symmetrical reflection geometry reflects the structural correlations in the orthogonal direction.

After intercalation by H_2SO_4 to give the stage-1 structure the equatorial anisotropy is still quite pronounced with the bulk of the H_2SO_4-PPV (200) peak (near $2\theta=18°$) and the $(1\bar{2}0)$ (near $2\theta=27°$) peak intensities oriented parallel and normal, respectively, to the film surface. Presuming that the layered structure is correct, this equatorial anisotropy can only be consistent with a model in which the H_2SO_4 galleries form along the direction normal to the film surface and, by construction, to that of the **a** lattice repeat of the PPV unit cell. This observation clearly invalidates any model that suggests intercalant gallery formation between [100] layers of the PPV chains. A more appropriate intercalation model requires, on average, alternating ± 1.3 Å (or $0.25b\sin\alpha$) shifts of the PPV chains parallel to the PPV $\mathbf{b}^*$ direction for the appearance of these galleries. Thus the PPV layers that appear in the doped phase structures are not the original ones present in the PPV host films.

IV. DISCUSSION AND CONCLUSION

In hindsight there are some features in this proposed scenario for formation of the stage-1 structure that are especially attractive. The transformation to the layered structure in Fig. 3(b) requires a highly anisotropic deformation of the PPV unit cell with a 1.7-Å contraction along the PPV $b\sin\alpha$ direction and a 6-Å expansion along the **a**-axis direction. Creation of intercalant galleries in the orthogonal direction, as shown in Fig. 3(d), requires a slightly smaller expansion of 5 Å and a much reduced *contraction* of 0.5 Å in the respective directions. Hence the second scenario involves a somewhat less dramatic global distortion of the polymer matrix. Furthermore, the creation of H_2SO_4 galleries along the lines of the first scenario would be naively expected to maintain the integrity of the staggered packing of PPV chains within the **b**-**c** plane (which gives rise to the monoclinic unit cell having an $\alpha\approx 135°$) and not overly reduce the unit cell coherence along the **b** direction. Experimentally, the pronounced reduction in the measured coherence lengths, as inferred from the peak widths, appears to be relatively isotropic within the equatorial plane and the well-defined PPV monoclinic unit cell angle α is not retained in the H_2SO_4-PPV stage-1 structure.

There are implications for the transport properties as well. The presence of closely spaced well-defined PPV stacks will enhance interchain hopping and transport perpendicular to the chain axis. The pronounced reconstructive nature of the stage-1 layer formation in combination with a high degree of structural disorder almost guarantees that individual PPV chains are strongly interconnected with adjacent layers

thereby leading to an anisotropic 3D metal system. Since only a single doped phase structure is observed, it is likely that sample aging[24] causes a progressive loss of the stage-1 fraction, which then reverts back to an undoped state. Since the majority of the intercalant layers are oriented perpendicular to the surface, the diffusion of H_2SO_4 out of the PPV films may be expected to be more readily facilitated. Further investigation of aged samples is necessary to adequately address these latter issues. Preliminary scattering data from fully dedoped PPV films suggest a strong recovery to the herringbone structure with a final crystal size intermediate to the original PPV films and that of the stage-1 structure.

In conclusion, we have confirmed by rigorous structure factor refinement that a stage-1 layer model is fully consistent with the available experimental data. More importantly, these experimental data point to a structural evolution in which the layer formation occurs by insertion of intercalant galleries parallel to the PPV **a-c** planes. It is possible that this behavior may extend to the stage-1 phases of other linear, unsubstituted conducting polymer hosts, although, given the subtle and often surprising diversity of structural response, it is unlikely that the model proposed here represents a universal intercalation theme in the formation of the polymer layer compounds.

ACKNOWLEDGMENTS

We gratefully acknowledge the support of this work through NSF Grant No. DMR-9631575 (G.M. and M.J.W.) and by the AFOSR (F.E.K.).

[1] *Science and Applications of Conducting Polymers*, edited by W. R. Salaneck, D. T. Clark, and E. J. Samuelsen (Hilger, Bristol, 1991).

[2] For a general review see the *Handbook of Conducting Polymers, 2nd ed.*, edited by J. R. Reynolds, R. Elsenbaumer, and T. Skotheim (Dekker, New York, 1997).

[3] R. Baughman, L. W. Shacklette, N. S. Murthy, G. G. Miller, and R. L. Elsenbaumer, Mol. Cryst. Liq. Cryst. **118**, 253 (1985).

[4] J. P. Aimé, M. Bertault, P. Delannoy, R. L. Elsenbaumer, G. G. Miller, and M. Schott, J. Phys. (France) Lett. **46**, L379 (1985).

[5] S. Flandrios, C. Hauw, and B. Francois, Mol. Cryst. Liq. Cryst. **117**, 91 (1985).

[6] F. Saldi, M. LeLaurain, and D. Billaud, Solid State Commun. **76**, 595 (1990).

[7] F. Saldi, J. Ghanbaja, D. Begin, M. LeLaurain, and D. Billaud, C.R. Acad. Sci., Ser. II: Mec., Phys., Chim., Sci. Terre Univers **309**, 671 (1989).

[8] M. J. Winokur, Y. B. Moon, A. J. Heeger, J. Barker, D. C. Bott, and H. Shirakawa, Phys. Rev. Lett. **58**, 2329 (1987).

[9] J. Ma, D. Djurado, J. E. Fischer, and P. A. Heiney, Phys. Rev. B **41**, 2971 (1990).

[10] P. A. Heiney *et al.*, Phys. Rev. B **44**, 2507 (1991).

[11] D. Djurado, J. E. Fischer, P. A. Heiney, J. Ma, N. Coustel, and P. Bernier, Synth. Met. **34**, 683 (1990).

[12] D. Chen, M. J. Winokur, Y. Cao, A. J. Heeger, and F. E. Karasz, Phys. Rev. B **45**, 2035 (1992).

[13] D. Chen, M. J. Winokur, and F. E. Karasz, Synth. Met. **41**, 341 (1991).

[14] G. Mao, M. J. Winokur, and F. E. Karasz, Phys. Rev. B **53**, R463 (1996).

[15] H.-Y. Choi, A. B. Harris, and E. J. Mele, Phys. Rev. B **40**, 3766 (1989).

[16] H.-Y. Choi and E. J. Mele, Phys. Rev. B **40**, 3439 (1989).

[17] A. B. Harris, Phys. Rev. B **50**, 12 441 (1994).

[18] J. P. Pouget, Z. Oblakowski, Y. Nogami, P. A. Albouy, M. Laridjani, E. J. Oh, Y. Min, A. G. MacDiarmid, J. Tsukamoto, T. Ishiguro, and A. J. Epstein, Synth. Met. **193**, 131 (1994).

[19] J. P. Pouget, P. Robin, R. Comes, H. W. Gibson, A.J. Epstein, and D. Billaud, Physica B & C **127B**, 158 (1984).

[20] G. Wieners, R. Weizenhofer, M. Monkenbusch, M. Stamm, G. Lieser, V. Enkelmann, and G. Wegner, Makromol. Chem. **6**, 425 (1985).

[21] M. A. Masse, J. B. Schlenoff, F. E. Karasz, and E. L. Thomas, J. Polym. Sci., Part B: Polym. Phys. **27**, 2045 (1989).

[22] W. Luzny, E. Samuelsen, D Djurado, and Y. Nicoulau, Synth. Met. **90**, 19 (1997).

[23] M. Reghu, Y. Cao, D. Moses, and A. J. Heeger, Phys. Rev. B **47**, 1758 (1993).

[24] M. Ahlskog, R. Menon, A. Heeger, T. Noguchi, and T. Ohnishi, Phys. Rev. B **55**, 6777 (1997).

[25] M. Dresselhaus and G. Dresselhaus, Adv. Phys. **30**, 139 (1981).

[26] S. Safran, in *Solid State Physics*, edited by F. Seitz, D. Turnbull, and H. Ehrenreich (Academic, London, 1987), Vol. 40, p. 187.

[27] R. H. Baughman, S. L. Hsu, G. P. Pez, and A. J. Signorelli, J. Chem. Phys. **68**, 5405 (1978).

[28] P. Robin, J. P. Pouget, R. Comes, H. W. Gibson, and A. J. Epstein, Polymer **24**, 1558 (1983).

[29] J. P. Pouget, in *Electronic Properties of Polymers and Related Compounds*, Springer Series in Solid State Science Vol. 64 (Springer, Heidelberg, 1985), p. 26.

[30] D. R. Gagnon, J. D. Capistran, F. E. Karasz, R. W. Lenz, and S. Antoun, Polymer **28**, 567 (1987).

[31] D. Chen, M. J. Winokur, M. A. Masse, and F. E. Karasz, Polymer **33**, 3116 (1992).

[32] Guomin Mao, Ph.D. thesis, University of Wisconsin, 1997.

[33] P. J. C. Smith and S. Arnott, Acta Crystallogr., Sect. A: Cryst. Phys., Diffr., Theor. Gen. Crystallogr. **A34**, 3 (1978).

[34] L. E. Alexander, *X-ray Diffraction Methods in Polymer Science* (Wiley-Interscience, New York, 1969).

[35] T. J. Prosa, M. J. Winokur, J. Moulton, P. Smith, and A. J. Heeger, Macromolecules **25**, 4364 (1992).

[36] G. Mao, J. E. Fischer, F. E. Karasz, and M. J. Winokur, J. Chem. Phys. **98**, 712 (1993).

[37] T. Granier, E. L. Thomas, D. R. Gagnon, J. R. W. Lenz, and F. E. Karasz, J. Polym. Sci., Polym. Phys. Ed. **24**, 2793 (1986).

[38] D. D. C. Bradley, R. H. Friend, T. Hartmann, E. A. Marseglia, M. M. Sokolowski, and P. D. Townsend, Synth. Met. **17**, 473 (1987).

[39] T. Granier, E. L. Thomas, and F. E. Karasz, J. Polym. Sci., Part B: Polym. Phys. **27**, 469 (1989).

[40] A. Macdiarmid and A. Heeger, Synth. Met. **1**, 101 (1979).

[41] M. Masse, Ph.D. thesis, University of Massachusetts, 1989.